ChemPubSoc Europe

DOI: 10.1002/cmdc.201500467

CHEMMEDCHEM Full Papers

SPECIAL ISSUE

Combined Use of Oligopeptides, Fragment Libraries, and Natural Compounds: A Comprehensive Approach To Sample the Druggability of Vascular Endothelial Growth Factor

Núria Bayó-Puxan,[a] Ricard Rodríguez-Mias,[a] Michael Goldflam,[a] Martin Kotev,[a] Sonia Ciudad,[a] Christopher J. Hipolito,[b] Monica Varese,[a] Hiroaki Suga,[b] Ramón Campos-Olivas,[c] Xavier Barril,[d, e, f] Víctor Guallar,[f, g] Meritxell Teixidó,[a] Jesús García,[a] and Ernest Giralt*[a, h]

The modulation of protein–protein interactions (PPIs) is emerging as a highly promising tool to fight diseases. However, whereas an increasing number of compounds are able to disrupt peptide-mediated PPIs efficiently, the inhibition of domain–domain PPIs appears to be much more challenging. Herein, we report our results related to the interaction between vascular endothelial growth factor (VEGF) and its receptor (VEGFR). The VEGF–VEGFR interaction is a typical domain–domain PPI that is highly relevant for the treatment of cancer and some retinopathies. Our final goal was to identify ligands able to bind VEGF at the region used by the growth factor to interact with its receptor. We undertook an extensive study, combining a variety of experimental approaches, including NMR-spectroscopy-based screening of small organic fragments, peptide libraries, and medicinal plant extracts. The key feature of the successful ligands that emerged from this study was their capacity to expose hydrophobic functional groups able to interact with the hydrophobic hot spots at the interacting VEGF surface patch.

[a] Dr. N. Bayó-Puxan,[+] Dr. R. Rodríguez-Mias,[+] Dr. M. Goldflam,[+] Dr. M. Kotev, S. Ciudad, Dr. M. Varese, Dr. M. Teixidó, Dr. J. García, Prof. E. Giralt
Institute for Research in Biomedicine (IRB Barcelona)
The Barcelona Institute of Science and Technology, Barcelona 08028 (Spain)
E-mail: ernest.giralt@irbbarcelona.org

[b] Dr. C. J. Hipolito, Prof. H. Suga
Department of Chemistry, Graduate School of Science
The University of Tokyo, Tokyo 113-8654 (Japan)

[c] Dr. R. Campos-Olivas
Spanish National Cancer Research, Madrid 28029 (Spain)

[d] Dr. X. Barril
Department of Physical Chemistry, University of Barcelona
Barcelona 08028 (Spain)

[e] Dr. X. Barril
The Institute of Biomedicine of the University of Barcelona
Barcelona 08007 (Spain)

[f] Dr. X. Barril, Prof. V. Guallar
Catalan Institution for Research and Advanced Studies
Barcelona 08010 (Spain)

[g] Prof. V. Guallar
Department of Life Sciences
Barcelona Supercomputing Center, Barcelona 08034 (Spain)

[h] Prof. E. Giralt
Department of Organic Chemistry
University of Barcelona, Barcelona 08028 (Spain)

[+] These authors contributed equally to this work.

Supporting Information for this article is available on the WWW under http://dx.doi.org/10.1002/cmdc.201500467.

SPECIAL ISSUE

This article is part of a Special Issue on Protein–Protein Interactions. To view the complete issue, visit: http://onlinelibrary.wiley.com/doi/10.1002/cmdc.v11.8/issuetoc.

Introduction

Protein–protein interactions

Proper cellular behavior is governed by a large map of interactions between various protein partners, the so-called interactome.[1] Research into protein–protein interactions (PPIs) has emerged as an important and challenging field in chemical biology and medicinal chemistry.[2] New and classical screening approaches in combination with medicinal chemistry have brought more than 12 small-molecule PPI modulators into clinical development, and it is expected that the market for this class of compounds will reach 600 million EUR in the next five years.[3] However, the design of molecules that interfere with these interactions is hindered by the size and topology of protein–protein interfaces. The surface of many proteins has evolved to interact either with other proteins or with small molecules. The contact area in a protein–protein interface is considerably larger (1500–3000 Å^2) than the average contact surface in the interaction between proteins and small molecules (300–1000 Å^2).[4] In addition, protein–protein interfaces tend to be flat and often lack the grooves or cavities[4] normally present in protein surfaces involved in the binding of small molecules. These considerations led to the concept of protein "druggability" coined by Hopkins and Groom.[5] Despite the large size of protein–protein interfaces, early studies revealed that not all interfacial residues contribute equally to complex stability.[6] A small subset of critical residues, called hot spots,[7] are responsible for a large fraction of the binding free energy. It has also been pointed out that large PPIs are often dominated by hot segments, which are continuous peptide stretches

that contribute the most to the binding interaction energy.[8] These observations have important implications for the development of small-molecule inhibitors of PPIs. These interactions have been traditionally considered as targets with low druggability potential. However, targeting hot spots or predominant hot segments makes it potentially feasible to disrupt PPIs by means of small- or medium-sized molecules.

VEGF–VEGFR: a therapeutically relevant protein–protein interaction system

Vascular endothelial growth factor (VEGF or VEGF-A) is probably the most important soluble factor involved in tumor angiogenesis.[9,10] VEGF belongs to the PDFG supergene family, which in mammals also includes VEGF-B, -C, -D, and -E, with which the former shares a varying degree of homology. VEGF is a glycoprotein expressed in various spliced isoforms ranging from 121 to 206 residues in length, and its 165-amino acid isoform is the most abundant. All these isoforms share a common homodimeric N-terminal receptor binding domain that has the ability to bind three tyrosine kinase receptors, namely, VEGFR-1 (also known as Flt-1), VEGFR-2, and VEGFR-3.[11] VEGF monomers are arranged in an antiparallel manner and are covalently linked by two symmetrical intermonomer disulfide bridges between Cys51 and Cys60. The monomer structure is characterized by a four-stranded central β sheet (i.e., strands β1, β3, β5, and β6) that is stabilized by a cystine knot motif formed by three intramolecular disulfide bonds (i.e., Cys26–Cys68, Cys57–Cys102, and Cys61–Cys104) at one end and by a small hydrophobic core at the opposite end. The structure also contains three additional short β strands (i.e., β2, β4, and β7) and two α-helical segments (i.e., α1 and α2).[12] Two symmetric receptor binding surfaces at the poles of the VEGF homodimer have been identified by mutational and structural studies.[13] The crystal structure of the VEGF–VEGFR-1 complex[14] revealed that no major conformational changes occur on VEGF upon receptor binding and that the intermolecular interaction is mediated mainly by hydrophobic contacts. Both X-ray[12] and NMR spectroscopy studies[15] suggest that the receptor binding region of VEGF has intrinsic conformational flexibility. Such flexibility may have important functional implications that allow the protein to interact with multiple receptors.

VEGF is overexpressed in most tumors and has a direct effect on sprouting angiogenesis.[16] It also acts as a survival factor by enhancing the expression of anti-apoptotic factors such as Bcl-2.[17] In general, VEGF induces receptor dimerization and activation of its kinase activity through autophosphorylation, which triggers a series of intracellular signaling pathways; it also sets off several processes common to other growth factors, namely, cell migration, survival, and proliferation.[18]

VEGF is particularly interesting as a therapeutic target because it acts directly on genetically stable endothelial cells rather than on tumor cells. Therefore, drugs that target VEGF are less prone to induce mutation selection on tumor cells and ultimately confer them with drug resistance.[19] VEGF inhibition suppresses tumor growth in animal models.[20] VEGF has also been identified as a key target to mitigate the effects of both wet age-related macular degeneration (AMD) and diabetes macular edema (DME), which are vision-limiting complications of aging and diabetes, respectively. DME affects nearly 30% of diabetes patients, whereas AMD is the main cause of permanent vision loss in the elderly.[21] High concentrations of VEGF have been correlated with chronic retinal microvascular damage. To date, 11 drugs that disrupt VEGF signaling have been approved for the treatment of several cancer types[22] and diseases related to macular degeneration.[23] Of these, seven (i.e., sunitinib,[24,25] sorafenib,[26,27] pazopanib,[28,29] vandetabnib,[30] axitinib,[31] regorafenib,[32] and cabozantinib[33]) are small molecules that inhibit the intracellular tyrosine kinase activity of the receptor. Of the remaining four drugs, two are monoclonal antibodies targeting either circulating VEGF (i.e., bevacizumab[34]) or the soluble extracellular fraction of the VEGF receptor (i.e., ramucirumab[35,36]). In addition, a chimeric fusion protein (i.e., aflibercept[37]) and an aptamer (i.e., pegaptanib[38]) have been described to block VEGF.

Recently, a small molecule interacting with the VEGFR-1 D2 domain and preventing VEGF binding was reported.[39] In the present study, we explored the capacity of small molecules to directly target the VEGF protein. The results of screening peptide and fragment-based libraries and plant extracts are discussed.

Results

We tackled the discovery of VEGF ligands by using several experimental approaches, including fragment screening, design and evaluation of linear and cyclic peptide libraries, and screening of plant extracts used in traditional Chinese medicine. We focused our methodology on the use of NMR spectroscopy, including the implementation of a highly efficient chemical shift perturbation (CSP) method based on methyl-^{13}C-Methionine selective labeling of VEGF. Computational chemistry was used to assist the screening process and was used to facilitate interpretation of the results.

Selective methyl-^{13}C-methionine-labeled VEGF for binding studies

$VEGF_{11-109}$ (from now on VEGF), a construct comprising residues 11–109 and containing the structured homodimeric N-terminal receptor binding domain, was chosen because its expression procedure and its backbone assignment have already been described.[15] By using ^{1}H–^{15}N HSQC NMR spectroscopy experiments, a uniformly ^{15}N-labeled VEGF sample was used to confirm both its fold integrity and its capacity to interact with v107, a peptide that binds with high affinity to the same region of VEGF that interacts with the VEGF receptor.[40] In the presence of v107, considerable changes in more than 50% of the VEGF NH resonances were observed (results not shown). Receptor-based ^{1}H–^{15}N HSQC experiments provide information about the most probable localization of ligand–protein interactions, which can be correlated to their biological functional effects. However, given the dramatic effects of v107 binding in the VEGF ^{1}H–^{15}N HSQC spectra, the interpretation of CSPs may

be misleading. Moreover, this method may be expensive and time consuming for a high-throughput screening strategy. Alternatively, in our screen of potential VEGF binders, we routinely used one-dimensional ligand-observed techniques such as saturation transfer difference (STD)[41] and WaterLOGSY experiments,[42] T_2-relaxation edited experiments,[43] and ^{19}F NMR spectroscopy.[44] However, these techniques also have some limitations. In particular, for complex mixtures, such as plant extracts, deconvolution of the contribution of each individual component may be challenging. In addition, NMR spectroscopy methods based on the existence of a fast equilibrium between the bound and free ligands may not be able to detect strong binders. Therefore, we focused our efforts on designing a cost-effective and time-efficient screening method that preserved the relevant mapping information. One way to achieve this goal is the NMR observation of specifically labeled side-chain resonances of the target protein. This approach has the potential to improve both the sensitivity and spectral resolution of the NMR spectra. Moreover, as side chains are less prone to long-range CSP effects, they may be more reliable than amide signals for the extraction of structural information.

The mode of interaction of VEGF with its receptors[14,45] and several peptides[40,46,47] was extensively studied and structurally characterized. Of the five VEGF methionine residues, two (i.e., Met18 and Met81) participate in the interaction with either v107 or VEGFR-1 and become deeply buried in the complex interface. Therefore, incorporation of selectively labeled methionine residues may enable the study of the intermolecular interactions of VEGF. The presence of three methionine residues (i.e., Met55, Met78, and Met94) outside the interface could provide extra information about the specificity of the interaction. The use of methionine as a labeling probe presents several additional advantages. Incorporation of commercially available methyl-^{13}C-methionine into proteins can be easily accomplished by using methionine auxotrophic *E. coli* strains. These strains are widely used in protein crystallography to solve the phase problem by using selenomethionine.[48] The labeling procedure is cost effective as only 80 mg of methyl-^{13}C-methionine (~300 € g^{-1}) per liter of growth media is required. Most importantly, ^{13}C-labeled methyl groups show high sensitivity and favorable NMR relaxation properties.[49] The combined use of methionine isotopic labeling and NMR spectroscopy detection was previously described for a carboxymethylated enzyme[50] and for in-cell NMR spectroscopy experiments.[51]

Methyl-^{13}C-Met-labeled VEGF was obtained following the procedure described for uniformly ^{15}N-labeled VEGF,[52] except that the methionine auxotrophic *E. coli* B834 strain was used and the minimal medium for cell growth was supplemented with methyl-^{13}C-Methionine. The protein yield was not greatly affected by the use of auxotrophic cells. Selectively methyl-^{13}C-Met-labeled VEGF displayed the expected five correlation signals in the ^{1}H–^{13}C HSQC NMR spectra (Figure 1). The addition of v107 revealed that, as expected, the most affected signals corresponded to methyl groups in Met18 and Met81. The largest change was detected on Met18, probably as a result of considerable contacts with Trp13 of v107 and the effect of its aromatic ring currents. The remaining methionine residues (i.e., Met55, Met78, and Met94) were virtually unaffected by v107.

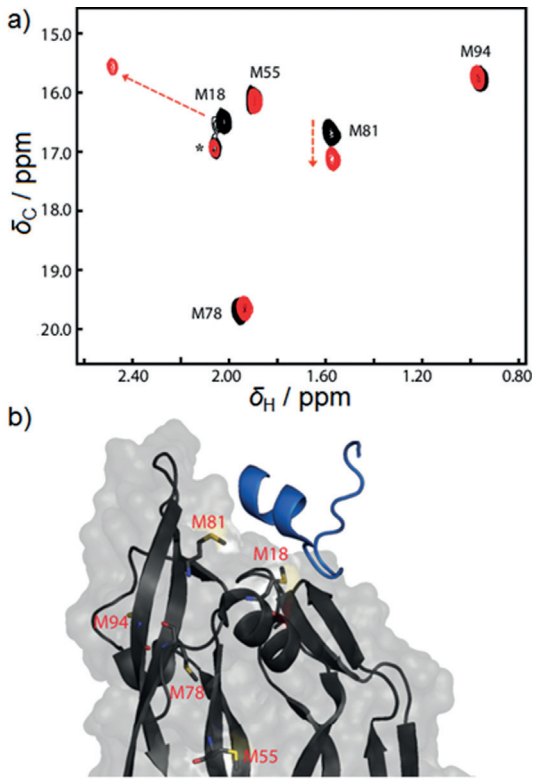

Figure 1. a) Comparison of the ^{1}H–^{13}C HSQC spectra of methyl-^{13}C-Met labeled VEGF (250 μM) in the absence (black) and in the presence of 2 equivalents of peptide v107 (red). The $(His)_6$-VEGF fusion protein used in this experiment contains a methionine outside of the VEGF sequence that is encoded by the starting codon of the gene expressing the fusion protein. An asterisk marks the cross signals of the $(His)_6$-VEGF initial Met. b) Expanded view of the structure of the VEGF–v107 complex (PDB ID: 1KAT). Homodimeric VEGF and v107 are shown in gray and blue, respectively. Methionine residues of VEGF are shown as stick models.

Evaluation of linear and cyclic oligopeptides

Oligopeptides can be considered privileged structures to modulate PPIs given that their chemical structure is identical to that involved in PPI interfaces. In addition, they are modular compounds, they cover a large chemical space, and they can be easily synthesized.

We designed two groups of all-D dipeptides. The first one was inspired in the retro-enantioversion[53] of peptide v107, which was dissected into a series of 20 dipeptides (Table 1). The second group of 6 peptides was composed by combining a representative set of amino acids, including Ala, Ile, Trp, Glu, Arg, and Ser (Table 1).

All-D dipeptides were evaluated against VEGF by STD and WaterLOGSY experiments. However, after extensive exploration of a series of experimental parameters (e.g., protein and ligand concentration, number of scans, saturation time, and saturation frequency), none of the all-D dipeptides seemed to bind VEGF.

Table 1. All-D dipeptide library.

Dipeptides based on the retroenantio version of v107			Ala-, Ile-, Ser-, Glu-, Arg-, and Trp-containing dipeptides	
N term.	Dipeptide[a]		N term.	Dipeptide[a,b]
H- Ac-	D-Leu-D-Arg D-Arg-D-Glu D-Glu-D-Phe D-Glu-D-Trp D-Trp-D-Glu	D-Trp-D-Met D-Met-D-Arg D-Arg-D-Ala D-Ala-D-Ile D-Ile-D-Asp	H-	D-Ala-D-Xaa D-Ile-D-Xaa D-Ser-D-Xaa D-Glu-D-Xaa D-Arg-D-Xaa D-Trp-D-Xaa

[a] Amide as C terminus. [b] Xaa = Ala, Ile, Ser, Glu, Arg, and Trp.

Under the hypothesis that the intrinsic flexibility of the all-D dipeptides analyzed may be detrimental for VEGF binding, we designed two symmetric cyclic hexapeptides containing chemically distinct dipeptide motifs, namely, Trp-Glu and Ile-Arg. A D-proline was included to facilitate cyclization and to confer conformational rigidity to the peptide structure. Cyclopeptides &D-Pro-Trp-Glu-D-Pro-Trp-Glu& and &D-Pro-Ile-Arg-D-Pro-Ile-Arg& were obtained by means of 9-fluorenylmethoxycarbonyl (Fmoc)/*t*Bu peptide chemistry on a solid support (see the Supporting Information). The capacity of the cyclic peptides to interact with VEGF was monitored by a combination of STD and protein-based CSP experiments by using a methyl-^{13}C-Met-labeled VEGF sample. Evidence of binding was only observed for the Trp-Glu-containing cyclic hexapeptide (Figure 2). In the presence of the Trp-Glu-containing cyclic hexapeptide, selective CSPs were induced in the two VEGF methionine residues (i.e., Met18 and Met81) located in the receptor interface, whereas the remaining methionine residues were almost unaffected. Titration experiments indicated that the Trp-Glu-containing cyclic hexapeptide binds VEGF in the low-millimolar range.

These promising results encouraged us to evaluate a massive library of cyclic peptides to explore a broader range of sequences and cycle sizes. For this purpose, we used a recently developed in vitro selection technology referred to as RaPID (random nonstandard peptide integrated discovery) system.[54] The RaPID system combines an RNA display method with flexible in vitro translation (FIT) technology used for the production of nonstandard peptides.[55,56] With this methodology, specific sequences of nonstandard peptides can be ribosomally expressed according to their mRNA templates.[57] The FIT system has been applied to the synthesis of a wide variety of Xaa-tRNAs, for which Xaa represents proteinogenic and nonproteinogenic amino acids[58–62] (see the Supporting Information). The selection on the mRNA display technology was performed with a mRNA library encoding for peptides from 5 to 15 amino acids with random sequences and showed enrichment of specific motifs (see the Supporting Information). The 10 macrocyclic peptides with the highest score were synthesized. Five of them were prepared as fluorescein-labeled compounds (Table 2). Macrocyclic peptides were synthesized by using Fmoc/*t*Bu peptide chemistry on a solid support. They were obtained in low yields (< 1%), which could be attributed to the high frequency of bulky 2,2,4,6,7-pentamethyldihydrobenzofuran-5-sulfonyl (Pbf)-protected arginine and β-branched amino acids and to the presence of multiple conformations of the final macrocycle.

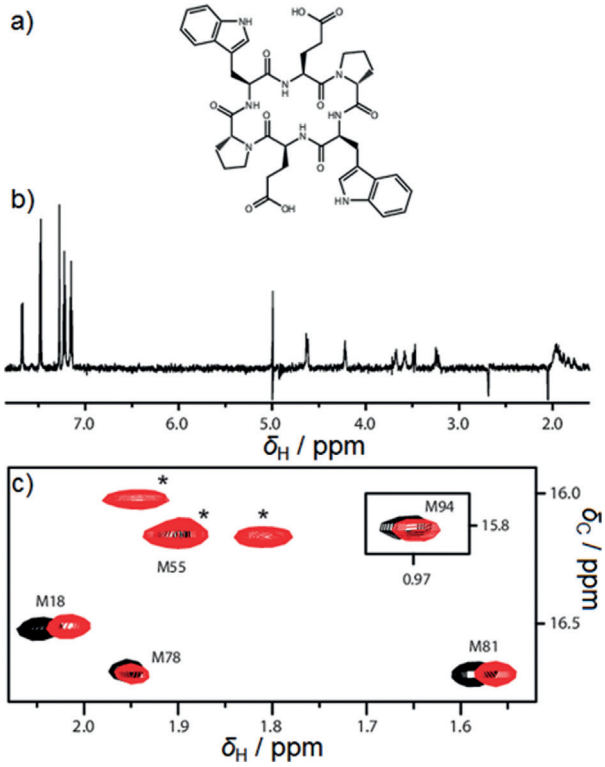

Figure 2. a) Chemical structure of the cyclic hexapeptide &D-Pro-Trp-Glu-D-Pro-Trp-Glu&. b) STD NMR spectrum (T = 278 K) of a sample containing 1 mM cyclic hexapeptide &D-Pro-Trp-Glu-D-Pro-Trp-Glu& and 10 μM VEGF. c) Overlay of the ^{1}H–^{13}C HSQC spectra (T = 318 K) of methyl-^{13}C-Met-labeled VEGF (50 μM) in the absence (black) and in the presence of 2.5 mM cyclopeptide &D-Pro-Trp-Glu-D-Pro-Trp-Glu& (red). The cross signals of Met78 are folded. Resonances corresponding to ^{13}C natural abundance peptide are marked by an asterisk.

Table 2. Macrocyclic peptides designed from the mRNA display technology.

Peptide	Sequence[a]	Purity [%]
1	fPKYRILYVRRRKP**C**GS	> 95
2	fRYYIVLKRRRTRIS**C**GS	> 95
3	FRRYR**C**YKVYTFTVKC*GS	> 95
4	FR**C**RRRIKISYYYLAC*GS	> 95
5	wRR(Me)F**C**(Me)S(Me)(F)RRVVRPC*GS	> 95
6	fRYAFWKIRYYKPSV**C**aK-fluorescein	> 95
7	fRYTTFTAVFLFRDR**C**GaK-fluorescein	> 95
8	fWTYYLIVSKSRNPH**C**aK-fluorescein	87
9	fKKTTIWRIRWTTRK**C**aK-fluorescein	80
10	FRSYSRRGRTWTYH**C**SK-fluorescein	> 95

[a] Small letters indicate non-natural amino acids: f = D-Phe; w = D-Trp; a = β-alanine; (Me) stands for *N*-methylamino acids; bold C indicates the location of the thioether bond to the N-terminal *N*-acetyl group. C* indicates the use of S-acetaminomethyl (Acm) side-chain protection.

The VEGF binding ability of unlabeled macrocyclic peptides (i.e., peptides **1**–**5**, Table 2) was evaluated by fluorescence polarization in a competitive assay with a previously described

fluorescent probe.[63] None of the tested peptides induced observable changes in the polarization signal of the probe (results not shown). These results suggest that either they do not bind to the protein interface with sufficient affinity to displace the tracer or they bind to other regions of the protein. Alternatively, fluorescent-labeled peptides (i.e., peptides **6**–**10**, Table 2) were assayed directly with VEGF to assess their interaction ability. However, none of the peptides showed any significant binding to VEGF.

Screening of fragment-based libraries

A fragment-based ligand discovery (FBLD) approach was selected, because it provides a highly effective way of exploring chemical space.[64–66] Fragment assembly allows access to very large numbers of potential fragment combinations. Although initial fragment hits are typically weak binders, two or more fragments can be covalently linked to yield medium-sized binders with higher affinity.

We used a chemical library that was designed by following a rational selection procedure from a catalog of more than 1.2 million compounds from several international vendors (e.g., Maybridge, Asinex and Enamine, Life Chemicals, Vitasmlab, and Specs). The design workflow is shown in Figure 3. All compounds in the library had commercial analogues to perform what Hubbard and collaborators referred to as a "structure and activity relationship (SAR) by catalog".[67] This concept implies that analogues from the original cluster can be ordered for each active fragment, which thus generates SAR data in a straightforward manner. A final library containing approximately 500 fragments, each one representing a large cluster, was built.

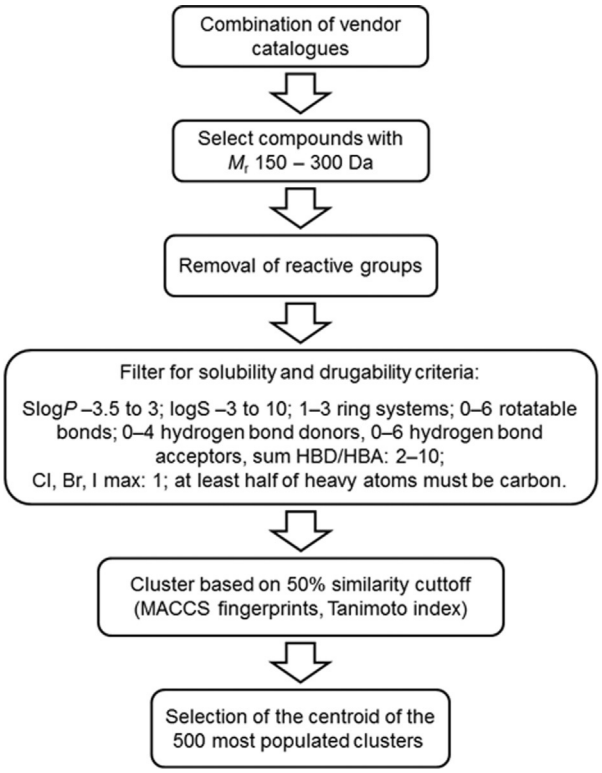

Figure 3. Overview of the strategy used for fragment selection.

To speed up the fragment screening, a previously described computational approach[68] was used to group compounds into cocktails that have minimized NMR signal overlap. This approach translates the NMR spectra of each compound into a computer-readable format (fingerprint) and then minimizes the global signal overlap by a SA (Monte–Carlo–Metropolis) algorithm. Using this algorithm, 81 five-fragment mixtures, containing a total of 402 compounds, were prepared. The fragment mixtures showed an average signal overlap of only 2%. Once assayed against VEGF by STD experiments, a group of potential VEGF binders (27%) was selected from the initial library. Then, we explored whether they were interacting at the expected site by using a competition STD experiment in the presence of v107. However, no evidence of displacement by v107 was observed for any of the fragments tested.

Alternatively, a reduced set of 100 compounds was tested in a ^{19}F NMR spectroscopy competition assay based on the displacement of a fluorinated "spy molecule" from the binding site of VEGF. For this purpose, a fluorinated v107-based peptide was designed and synthesized (see the Supporting Information). Two candidates seemed to partially compete with the spy peptide in the ^{19}F NMR spectroscopy assay. Unfortunately, binding of these fragments to VEGF could not be validated by protein-observed NMR spectroscopy techniques and they were discarded.

^{19}F NMR spectroscopy was also used to directly screen a previously described collection (FFCNIO library) of approximately 380 fluorinated compounds[69] against VEGF. They were grouped in eight-compound mixtures with non-overlapping ^{19}F NMR signals. We detected four low-affinity binders from the FFCNIO library in the primary cocktail screening (see the Supporting Information). However, none of these compounds behaved as an efficient and selective VEGF binder if studied in isolation.

Several computational approaches, including molecular docking and induced-fit docking calculations, were used to further evaluate the fragment-based approach. The SiteMap module of the Schrödinger Suite[70] identified four potentially druggable areas on the protein surface (i.e., sites 1, 2, 3, and 4 in Figure 4a). Remarkably, the protein region involved in receptor and v107 binding (i.e., site 5, Figure 4a) was not among the most "druggable" regions of VEGF. Next, by means of docking calculations by using XP Glide (Schrödinger),[70] we examined the previously mentioned fragment-based library of approximately 500 compounds (M_r: 150–300 Da). XP Glide docking also confirmed the SiteMap results and showed better binding options for sites 1 and 2 outside the receptor binding site (Figure 4b). Finally, the search for potential transient surface clefts by a protocol for induced-fit docking with Protein Energy Landscape Exploration (PELE)[71] did not predict any well-formed cleft in the receptor recognition region of VEGF. Taken together, these in silico studies suggested that the most probable binding regions of small fragments fall outside the receptor binding site of VEGF.

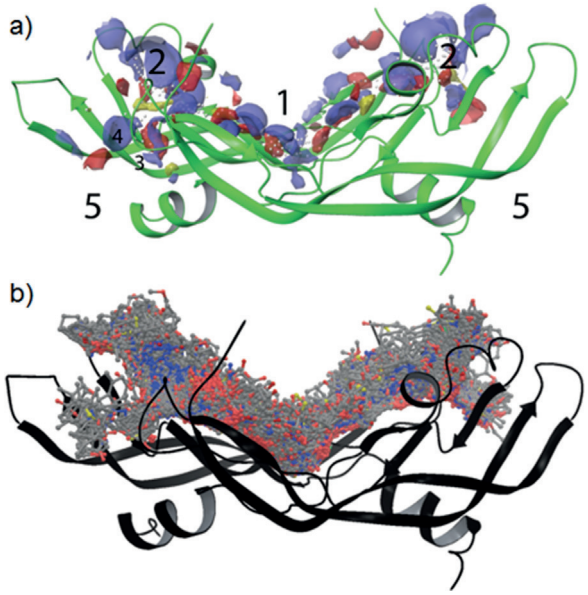

Figure 4. a) Analysis of the SiteMap computations reveals druggability mainly in the channel formed between the two chains of the VEGF homodimer (sites 1, 2, 3, and 4). Red, blue, and yellow surfaces show sites for potential H-bond acceptor, H-bond donor, and hydrophobic interactions, respectively. White dots indicate the presence of small cavities. Receptor binding sites are indicated by 5. The number size correlates with the size of the binding sites. b) Representation of the XP GLIDE docking results. A selected library of approximately 500 compounds (gray carbon atoms) was docked against the VEGF homodimer (black ribbons). Sites 1 and 2 (panel a) were most populated.

Natural compounds: flavonoids from medicinal plant extracts as VEGF binders

A considerable number of drugs that are currently used in cancer therapy are natural products or their derivatives.[72,73] In this regard, traditional medicinal plants offer enormous potential in the search for new potential drugs. Cancer is among the conditions treated by traditional herbal medicine. Interestingly, some of the antitumoral plants or compounds used in traditional medicine operate through an antiangiogenic mechanism, modulating one or various targets involved in vessel formation. From the literature on traditional Chinese medicine,[74] we selected a small subset of 50 plants for their high recurrence in medical prescriptions. Dried plant material was extracted with water by means of a Soxhlet apparatus. Given that VEGF only contains five methionine residues, protein-detected ^{13}C-filtered-^{13}C-decoupled ^{1}H NMR spectroscopy was used to detect potential VEGF binders. The spectra were obtained with a one-dimensional version of the ^{1}H–^{13}C HSQC pulse sequence, and they provided enough resolution to individually resolve the resonances of the VEGF methionine residues in a time-efficient manner. Identical experiments were acquired for free VEGF and for VEGF after the addition of mixtures of three different plant extracts. Two extract mixtures induced spectral changes in VEGF. Next, individual extracts from the positive mixtures were added to the protein. Small, yet dose-dependent, minor shifts were observed for Met18 and Met81 in the presence of extracts from *Medulla Junci* and *Radix scutellariae* (Figure 5). In both cases, the shifts observed were typical of weak binders in a fast exchange regime.

The chromatographic profiles of these extracts are shown in Figure 5. We pursued the isolation and characterization of the active compound(s) involved in VEGF binding. Using a combination of mass spectrometry and homonuclear (COSY and NOESY) and heteronuclear (^{1}H–^{13}C HSQC and HMBC) NMR spectroscopy techniques, the major component of the *R. scutellariae* extract was identified as baicalin[75] (Figure 6). We then confirmed that isolated baicalin was able to bind VEGF (Figures 5 and 6).

STD experiments were performed to identify the binding epitope of baicalin (Figure 6). Relative quantification of transferred saturation indicated that the most buried part of the molecule was the phenyl group, whereas the least saturated and consequently the most exposed part was the more hydrophilic glucuronic moiety. Finally, a STD competition assay with peptide v107 was performed. Increasing amounts of v107 were added to the baicalin–VEGF sample and subsequent STD experiments were recorded. As shown in Figure 6, these experiments revealed a stepwise reduction in the baicalin STD signals, which became undetectable in the presence of 100 μM peptide v107, which thereby indicated that baicalin and v107 compete for the same binding site.

The interaction of baicalin with VEGF was further characterized by ^{1}H–^{15}N HSQC experiments. Upon the addition of baicalin, the most remarkable CSPs were found in a region centered in residues 85–96. In addition, resonances corresponding to amino acids in the vicinity of positions 46–48 and 18–22 were also significantly shifted (Figure 7). Titrations were conducted and baicalin-induced CSPs in the VEGF spectra were quantified and used to determine the binding affinity; K_D values of 4.9 and 6.8 mM were obtained for ^{1}H–^{13}C HSQC and ^{1}H–^{15}N HSQC shifts, respectively (see the Supporting Information). Although baicalin is a weak binder, it provides a reasonable starting point to explore other structurally related, commercially available compounds.

A small set of several baicalin-related compounds were chosen (Figure 7a). These molecules conserve the flavone scaffold and show minor variations in the number and position of several aromatic hydroxy groups. Of these molecules, the glycosylated flavone quercetin-3-β-glucoside was the only one that induced methionine perturbations on the ^{13}C-filtered-^{13}C-decoupled ^{1}H NMR spectra of VEGF. Titration of VEGF with this glycosylated flavone provided a dissociation constant of ~2 mM, which suggests that quercetin-3-β-glucoside has a slightly higher affinity than baicalin for VEGF (see the Supporting Information). Comparison of the amide chemical shift changes of VEGF induced by quercetin-3-β-gluocoside and baicalin revealed several interesting trends (Figure 7b). First, in agreement with the differences in K_D values estimated for the two molecules, to produce similar chemical shift changes on VEGF, the concentration of baicalin required was approximately twice that required for quercetin-3-β-glucoside. Second, both compounds affected a common cluster of amino acids centered on Phe47, in addition to some residues close to the N-terminal α-helix 1, such as Met81 and Arg23. Beyond these

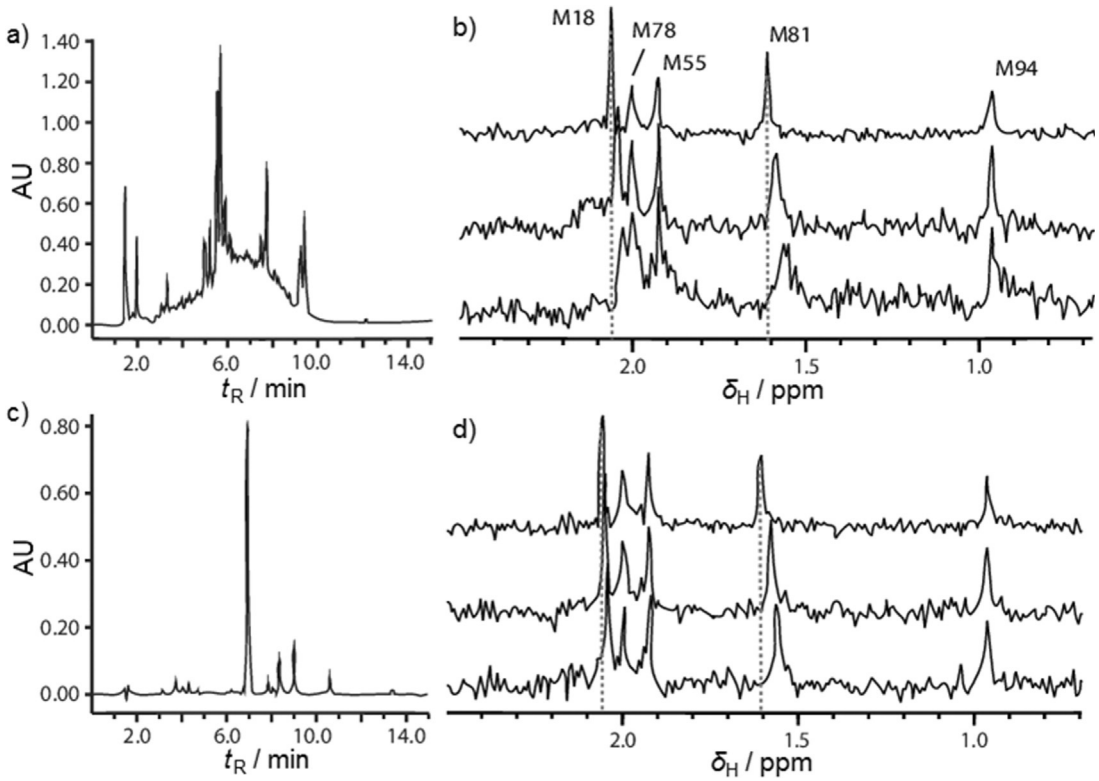

Figure 5. Chromatographic profile of representative water extracts of a) *Medulla Junci* and c) *Radix scutellariae*. ^{13}C-Filtered–^{13}C decoupled ^{1}H NMR spectra of a 30 μM methyl-^{13}C-Met-labeled VEGF sample in the absence (b and d, top) and in the presence of 3 μL (b and d, middle) and 6 μL (b and d, bottom) of a stock solution, prepared as described in the Experimental Section, of either b) *Medulla Junci* or d) *Radix scutellariae* extracts.

similarities, most of the changes produced by baicalin were concentrated around residues 86–93, located at β-strands 5 and 6 and their interconnecting loop. Conversely, quercetin-3-β-glucoside-specific perturbations were mainly located on the opposite site of VEGF, around Phe36 and the loop connecting to the second β strand. These observations suggest that baicalin and quercetin-3-β-glucoside target overlapping but slightly different sites on VEGF owing to their distinct binding orientations. Given that the two VEGF ligands share a common flavone scaffold and differ mainly in the type and location of the glycosidic moiety and to a lesser extent in the position of various hydroxy groups, it is reasonable to place the common scaffold on the locus of Phe47, the region equally affected by these two flavonoid analogues. This model is in agreement with the experimental STD data, which suggested that the binding contribution of the flavone scaffold was stronger than that of the glycosidic moiety. The glucuronic moiety of baicalin is most likely accommodated between α-helix 1 and β-strands 5 and 6, as residues in these secondary structure elements were selectively affected by baicalin. In contrast, the sugar moiety of quercetin-3-β-glucoside is probably located on the opposite site of the protein, which induces significant shifts on Gly65 and residues on α-helix 2 (Figure 7c). Overall, the screening of plant extracts from traditional Chinese medicine allowed us to identify a flavonoid scaffold that is able to bind VEGF in the VEGFR binding interface.

Discussion

The term "druggability" is used to describe a biological target that is known to bind with high affinity to a low molecular weight drug.[5] Many proteins, including several related to cancer, are considered as "undruggable" targets.[76] The only VEGF ligands that have found their way into clinical practice are monoclonal antibodies[34–36] and, more recently, aptamers.[38] In the present study, we summarized several years of work of many members of our research group, and also of several collaborators, in an effort to explore the feasibility of a therapeutic strategy based on blocking the VEGFR interaction by using ligands—other than biologics—able to bind VEGF specifically in the region of interaction with its receptor. Herein, we explored a wide variety of approaches, including NMR spectroscopy based fragment screening, screening of peptide libraries, and activity screening of plant extracts. This extensive work provided a clear picture. First, it was difficult to identify high-affinity ligands by using these approaches. Second, the only ligands (weak) that bind to the VEGF surface patch involved in the interaction with the receptor are conformationally restrained cyclic peptides and medium-sized natural products. Finally, all the small molecular weight organic fragments able to bind VEGF interact with the protein in patches other than the therapeutically relevant one.

This behavior, in particular the difficulties encountered to identify small organic fragments targeting the VEGF interacting surface, could be related to the topological and chemical fea-

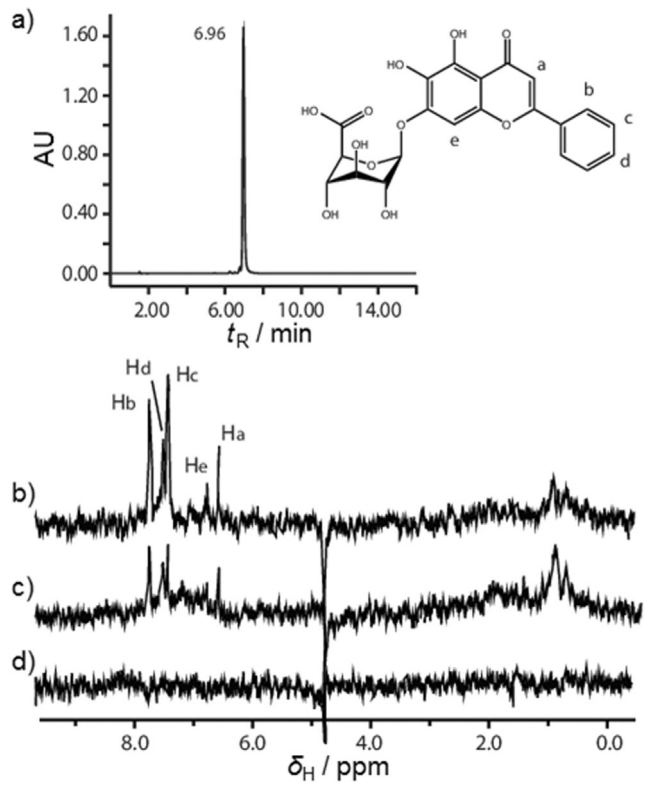

Figure 6. a) HPLC chromatogram of baicalin extracted from the *Radix scutellariae* plant extract. The chemical structure of baicalin is shown (right). b) STD NMR spectrum ($T = 298$ K) of a sample containing 1 mM baicalin and 10 μM VEGF. STD spectra of the same sample in the presence of c) 50 μM and d) 100 μM v107 peptide showing the reduction of the STD signal intensities of baicalin in the presence of v107.

tures of the protein–protein interface. The VEGF–VEGFR-1 binding interface is flat, mainly hydrophobic, and rather large (> 800 Å^2 per receptor unit),[13] which thereby suggests that targeting this interaction may be especially challenging. However, a compound interacting with the VEGF binding site in the VEGFR D2 domain and inhibiting complex formation was recently described.[39] This observation thus indicates that this PPI may be amenable to disruption by synthetic compounds. Several VEGF segments distant in sequence generate a discontinuous binding epitope that contributes to receptor binding. The binding determinants of VEGF for VEGFR are localized on the N-terminal α-helix 1 (residues 16–27), the loop connecting β3 to β4 (residues 61–66), and strand β7 (residues 103–106) of one VEGF monomer as well as strand β2 (residues 46–48) and strands β5 and β6, and the turn connecting them (residues 79–91).

Protein–protein interfaces could be structurally classified as domain–domain or peptide–domain interactions.[4] In domain–domain PPIs, two globular protein domains are involved in the interface, whereas in peptide-mediated PPIs a continuous polypeptide segment binds to a globular domain. The size and shape of the contact area differ considerably between the two interaction types. Peptide-mediated interfaces have relatively small contact areas with hot spot residues in close proximity. In addition, members of this class tend to contain defined pockets at the interface that may act as anchors of interacting residues. These structural features make peptide-mediated interactions more suited for inhibitors than the larger and flatter domain–domain interfaces.

An increasing collection of PPI inhibitors has been described.[8] Representative examples of successfully targeted PPI interactions include, among others, those of the p53 activation domain with MDM2,[77] Bcl-xL proteins with BH3 peptides,[78] and cytokine interleukin-2 IL2 with its receptor IL2Rα.[79] More recently, our research group reported a series of photoswitchable inhibitors of clathrin-mediated endocytosis able to disrupt the β-arrestin–β-adaptin 2 interaction.[80,81] Most targeted PPIs are either peptide–domain interactions or a fraction of domain–domain PPIs that contain a continuous dominant peptide at the interaction interface that contributes most of the binding energy. In the latter case, inhibitors often target the interface region in which the dominant peptide interacts.

The reasons why targeting VEGF has proven to be extremely challenging are probably correlated with the absence of desirable druggable features in VEGF. The VEGF–VEGFR interaction is a typical domain–domain interaction. VEGF contains a relatively flat and extended interface with hot spots distributed over a large area. The distance between the Cα of Leu66 and Met18 is ~20 Å. Using several computational techniques, we predicted the lack of preformed or transient cavities or clefts with potential capacity to bind small molecules with reasonable affinity in the receptor binding surface of VEGF.

The presence of large exposed hydrophobic surface patches is one of the signatures of domain–domain PPIs. In this context, our results suggest that to disrupt domain–domain PPIs ligands would need to expose hydrophobic surfaces that are over a minimal threshold. This requirement translates, on the one hand, into the need for a minimum molecular weight. On the other hand, conformational constraints are required to prevent these relatively large hydrophobic molecules to adopt energetically favored folded conformations that would shield the hydrophobic functional groups from the water. In other words, it would be necessary to force the hydrophobic parts of the molecule to remain exposed at the surface, which would thus facilitate interaction with the hydrophobic patch at the protein surface. Our analysis could be applicable to other targets of this nature and may help in the design of inhibitors and/or screening strategies of many therapeutically relevant domain–domain PPIs.

Experimental Section

Chemistry

Protein production: $VEGF_{11-109}$ (VEGF) was expressed, purified, and refolded as described in detail elsewhere.[53] Large-scale expression was performed on a 10 L scale with a Biostat B fermentor (Sartorius). In this case, protein expression was induced once the culture reached an optical density of 1.2 at 600 nm (OD_{600}), and cells were harvested at an OD_{600} of ~6.0. During the fermentation, oxygen was supplemented into gas flow and the pH was kept constant at 7.0.

Peptide synthesis: A standard solid-phase Fmoc/*t*Bu peptide synthesis protocol was followed. Dipeptide libraries were supplied by

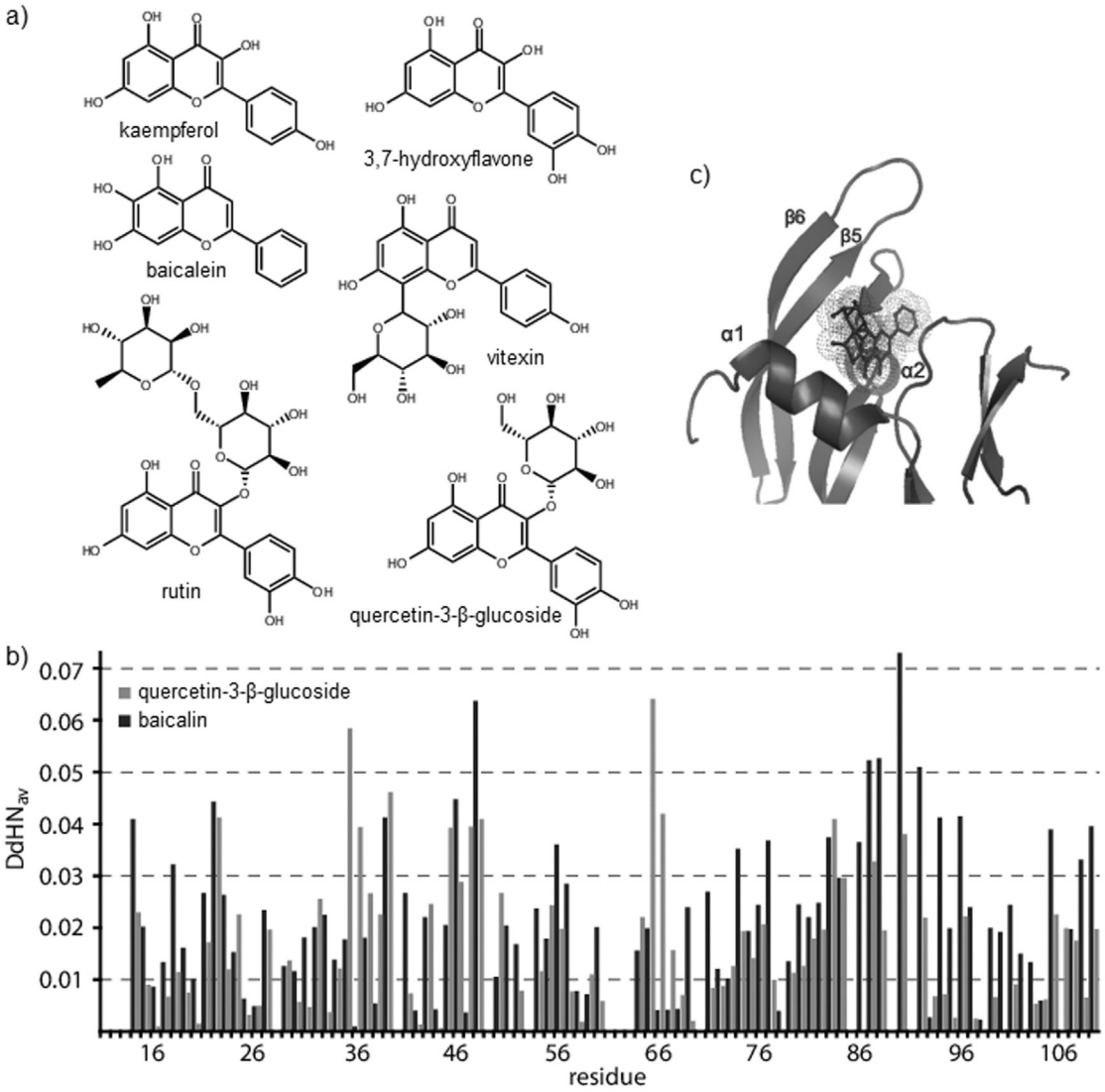

Figure 7. a) Chemical structure of the flavonoid molecules tested. b) Histogram showing weighted average chemical shift changes for VEGF amide resonances between free ^{15}N-labeled VEGF (250 μM) and ^{15}N-labeled VEGF (250 μM) in the presence of either 7.7 mM baicalin (black) or 4.4 mM quercetin-3-β-glucoside (gray). c) Model of the VEGF–baicalin complex. VEGF is shown as a cartoon representation and baicalin as a ball and stick model.

Dr. F. Yraola from the Combinatorial Chemistry Unit at the Barcelona Science Park. These libraries were produced by solid-phase synthesis and were purified by HPLC to a purity 95% or higher. For storage purposes, compounds were weighed and dissolved in [D_6]DMSO at a concentration of 100 mM.

For the synthesis of symmetric cyclic hexapeptide &D-Pro-Trp-Glu-D-Pro-Trp-Glu&, 2-chlorotrityl resin (CTC resin, 250 mg, 1.6 mmol g^{-1}) was placed in a 20 mL polypropylene syringe fitted with a polyethylene filter disc. The resin was then washed with CH_2Cl_2 (5×30 s) and a solution of Fmoc-L-Trp(Boc)-OH (184.3 mg, 0.7 equiv) and *N*,*N*-diisopropylethylamine (DIEA; 366 μL, 10 equiv) in CH_2Cl_2 was then added; the mixture was then stirred for 1 h at room temperature. The remaining active sites were capped with the addition of MeOH (400 μL), and the mixture was stirred for an additional 10 min at room temperature. The Fmoc-L-Trp(Boc)-O-CTC resin was subjected to the following washes: CH_2Cl_2 (5×30 s), DMF (5×30 s), and 20% piperidine in DMF (1×1 min, 2×5 min, 1×10 min). Elongation of the peptide was achieved by the sequential addition of Fmoc-AA-OH (3 equiv) with 2-(1*H*-7-azabenzotriazol-1-yl)-1,1,3,3-tetramethyluronoium hexafluorphosphate (HATU, 3 equiv) and DIEA (6 equiv) as coupling reagents in DMF. The coupling reaction was stirred for 30 min, and before filtration the corresponding colorimetric test (ninhydrin test for primary amines and chloranil test for secondary amines) was done to qualitative assess if coupling reactions were completed. Removal of the Fmoc group was performed with 20% piperidine in DMF (1×1 min, 2×10 min, 1×10 min). The H-Glu(O*t*Bu)-D-Pro-Trp(Boc)-Glu(O*t*Bu)-D-Pro-Trp(Boc)-O-CTC peptide resin was treated with 1% trifluoroacetic acid (TFA) in CH_2Cl_2 (5×30 s) to cleave the peptide from the resin. The filtrates were collected over H_2O (60 mL per gram of resin). CH_2Cl_2 was removed under an atmosphere of nitrogen and water was removed by lyophilization. The linear peptide was subjected to head-to-tail cyclization in solution by using (7-azabenzotriazol-1-yloxy)tris(pyrrolidino)phosphonium hexafluorophosphate (PyAOP) and DIEA as coupling reagents in a mixture of CH_2Cl_2/DMF (98:2) at high dilution (5 mM) for 16 h at room temperature. The cyclic peptide was treated with TFA/H_2O/triisopropylsilane (TIS) (95:2.5:2.5, *v*/*v*/*v*) for 2 h at room temperature to remove all protecting groups. Solvent was removed under an atmosphere of ni-

trogen, and the crude product was purified by CombiFlash automated flash chromatography (Teledyne ISCO) to obtain the final peptide (39.1 mg, 47%). ^{1}H NMR (600 MHz, H_2O/D_2O = 90:10): δ = 10.10 (s, 1H), 8.49 (d, J = 7.6 Hz, 1H), 7.70 (d, J = 8.1 Hz, 1H), 7.68 (d, J = 8.8 Hz, 2H), 7.49 (d, J = 8.5 Hz, 2H), 7.27 (s, 2H), 7.24 (t, J = 7.7 Hz, 2H), 7.16 (t, J = 7.7 Hz, 2H), 4.26–4.17 (m, 1H), 3.71–3.62 (m, 1H), 3.62–3.54 (m, 1H), 3.48 (dd, J = 15.6, 4.3 Hz, 1H), 3.22 (dd, J = 15.5, 9.5 Hz, 1H), 2.05–1.98 (m, 2H), 1.98–1.83 (m, 4H), 1.82–1.73 (m, 1H), 1.49–1.38 ppm (m, 1H). HPLC (solvent A: H_2O with 0.045% TFA, solvent B: MeCN with 0.036% TFA, conditions 7:3 to 0:10 in 15 min): t_R = 6.2 min. Purity: > 98%.

mRNA display-derived peptides: Chloroacetylation of the free N terminus was performed with a solution of 0.2 M Cl-Ac-NHS (NHS = *N*-hydroxysuccinimide; 2.5 mL) dissolved in *N*-methyl-2-pyrrolidone (NMP) under shaking for 40 min. For fluorescein conjugation, after chloroacetylation, the 4-methoxytrityl (Mmt) group was removed by acidic solution (TFA/TIS/CH_2Cl_2, 1:1:98, *v/v/v*) for 10 min. The peptidyl resin was then extensively washed with CH_2Cl_2 (3×1 min), NMP (3×1 min), 10% DIEA in NMP (3×1 min), and NMP (3×1 min). The peptidyl resin was subjected to a reaction with a solution of 0.1 M NHS-fluorescein in 10% DIPEA in NMP for 1 h at room temperature. Cleavage from the resin and removal of side-chain protecting groups was performed under stronger acidic conditions (TFA/TIS/1,2-ethanedithiol (EDT)/H_2O, 9.25:0.25:0.25:0.25, *v/v/v/v*) for 3 h at room temperature. After removal of TFA, the crude product was redissolved in DMSO (2.5 mL) and diluted with MeCN/H_2O (1:1, *v/v*, 1000 mL). The solution was adjusted to pH 9 with Et_3N to perform the head-to-side chain cyclization. The crude product was purified by HPLC. Table 3 shows the characterization data from the peptides obtained.

Table 3. Characterization of mRNA display-derived peptides.

Peptide	HPLC[a]	t_R [min]	Mass [*m/z*]	
			Expected	Found
1	100:0–0:100	4.8	1109.43 (z = 2)	1109.44 (z = 2)
2	100:0–0:100	4.1	771.77 (z = 3)	7771.77 (z = 3)
3	100:0–30:70	4.9	796.40 (z = 3)	796.40 (z = 3)
4	95:5–0:100	4.1	465.40 (z = 3)	765.40 (z = 3)
5	90:10–50:50	4.4	722.05 (z = 3)	722.05 (z = 3)
6	80:20–50:50	7.7	908.44 (z = 3)	908.44 (z = 3)
7	100:0–0:100	4.9	899.42 (z = 3)	899.42 (z = 3)
8	80:20–50:50[b]	10	870.74 (z = 3)	870.73 (z = 3)
9	80:20–20:80	3.9	907.47 (z = 3)	907.47 (z = 3)
10	90:10–60:40	5.5	647.79 (z = 4)	647.79 (z = 4)

[a] HPLC gradient (8 min); solvent A: H_2O + 0.045% TFA; solvent B: MeCN + 0.036% TFA [b] 15 min time gradient in a C_4 column (4.6 mm×15 mm).

Plant extracts from traditional Chinese medicine: Plants were obtained from Herbasin (Shenyang, China). Dried plant material (30 g) was extracted with H_2O (400 mL) at reflux for 5 h by means of a Soxhlet apparatus. The volume of the aqueous extracts was reduced by evaporation under vacuum, and the extract was then freeze dried. Finally, [D_6]DMSO stocks were prepared at a 200 mg mL^{-1} concentration.

NMR spectroscopy

STD and WaterLOGSY experiments were conducted over a range of temperatures (37, 25, or 5 °C) with Bruker Digital Avance 600 MHz and Varian Inova 500 MHz spectrometers. Samples contained 10 μM VEGF and 0.5 or 1 mM of assayed compound(s) in 25 mM sodium phosphate (pH 7.0), 50 mM NaCl, and 90% D_2O. On-resonance irradiation was performed on the water signal for WaterLOGSY experiments and on the aliphatic protein region for STD experiments. The total saturation time was 2–2.5 s, and water suppression was achieved with a watergate module.

In the screening experiments, fragments showing STD signals with "normal" or "strong" intensities for more than 30% of their protons were classified as potential good binders.

Two-dimensional ^{1}H–^{15}N HSQC and ^{1}H–^{13}C HSQC experiments and 1D ^{13}C-decoupled-^{13}C-filtered ^{1}H NMR spectra were usually obtained at 45 °C with a Bruker Avance III 600 MHz spectrometer equipped with a cryoprobe. Standard samples for protein-observed experiments contained 100–200 μM (^{1}H–^{15}N HSQC) or 30 μM (^{1}H–^{13}C HSQC and 1D ^{13}C-decoupled-^{13}C-filtered ^{1}H) VEGF in buffer A: 25 mM sodium phosphate (pH 7.0), 50 mM NaCl, and 10% D_2O. 2D ^{1}H–^{13}C HSQC experiments were typically acquired by using 256× 96 points and 8 scans per increment with spectral widths of 960 Hz (1.6 ppm) and 453 Hz (3.0 ppm) in the ^{1}H and ^{13}C dimensions, respectively. Using this ^{13}C spectral width, cross-signals of Met78 were folded. ^{13}C-decoupled-^{13}C-filtered ^{1}H NMR spectra were recorded with 2048 points, a spectral width of 9000 Hz and 128 scans.

^{1}H–^{15}N HSQC spectra were acquired with 1024 complex points in the F2 (^{1}H) dimension and 100 increments in the F1 (^{15}N) dimension, 96 scans for each increment, and a spectral width of 7212 Hz (12.0 ppm) in F2 and 1794 Hz (29.5 ppm) in F1.

The dependence of the chemical shift changes of VEGF on the ligand concentration was used to estimate binding constants. ^{1}H NMR and ^{15}N NMR chemical shift changes from ^{1}H–^{15}N HSQC titrations or alternatively ^{1}H NMR and ^{13}C NMR shifts from ^{1}H–^{13}C HSQC experiments were combined as previously described.[82] For ligands interacting in the receptor-binding site of VEGF, two equal and independent binding sites were assumed.[82]

All ^{19}F NMR spectra were acquired with a Bruker spectrometer operating at 700 MHz and equipped with a dual fluorine-proton SEF probehead and a robotic arm BACS120. The CF_3 and CF cocktail samples for the ^{19}F NMR screening were prepared at 20 and 50 μM, respectively, by diluting premixed cocktail stocks (10 mM each of the eight compounds in each stock) in [D_6]DMSO in a final volume of 550 μL of buffer A.

Two ^{19}F NMR spectra for each cocktail sample were recorded: a regular 1D and a 1D containing a CPMG T_2 filter of 200/400 ms (for CF/CF_3), before and after the addition of 2 μM VEGF. Spectra were recorded with a 20 Hz sample spinning using 128 scans, acquisition and recovery times of 1.2 s and 2.5 s, respectively, in 8.5–9.5 min per spectrum.

Acknowledgements

This work was supported by the Ministry of Economy and Competitiveness and the European Fund for Regional Development (MINECO-FEDER) (Bio2013-40716-R) and the Generalitat de Catalunya (XRB and 2014-SGR-521). We also thank the NMR facility at the Scientific and Technological Centre of the University of Barcelona (CCiT UB) for their technical support.

Keywords: drug discovery · fragment screening · growth factors · peptides · protein–protein interactions

[1] J. D. Han, D. Dupuy, N. Bertin, M. E. Cusick, M. Vidal, *Nat. Biotechnol.* **2005**, *23*, 839 – 844.
[2] M. R. Arkin, J. A. Wells, *Nat. Rev. Drug Discovery* **2004**, *3*, 301 – 317.
[3] T. L. Nero, C. J. Morton, J. K. Holien, J. Wielens, M. W. Parker, *Nat. Rev. Cancer* **2014**, *14*, 248 – 262.
[4] J. A. Wells, C. L. McClendon, *Nature* **2007**, *450*, 1001 – 1009.
[5] A. L. Hopkins, C. R. Groom, *Nat. Rev. Drug Discovery* **2002**, *1*, 727 – 730.
[6] T. Clackson, J. A. Wells, *Science* **1995**, *267*, 383 – 386.
[7] A. A. Bogan, K. S. Thorn, *J. Mol. Biol.* **1998**, *280*, 1 – 9.
[8] N. London, B. Raveh, O. Schueler-Furman, *Curr. Opin. Chem. Biol.* **2013**, *17*, 952 – 959.
[9] N. Ferrara, T. Davis-Smyth, *Endocr. Rev.* **1997**, *18*, 4 – 25.
[10] T. Torimura, M. Sata, T. Ueno, M. Kin, R. Tsuji, K. Suzaku, O. Hashimoto, H. Sugawara, K. Tanikawa, *Hum. Pathol.* **1998**, *29*, 986 – 991.
[11] N. Ferrara, H.-P. Gerber, J. LeCouter, *Nat. Med.* **2003**, *9*, 669 – 676.
[12] Y. A. Muller, H. W. Christinger, B. A. Keyt, A. M. de Vos, *Structure* **1997**, *5*, 1325 – 1338.
[13] Y. A. Muller, B. Li, H. W. Christinger, J. A. Wells, B. C. Cunningham, A. M. de Vos, *Proc. Natl. Acad. Sci. USA* **1997**, *94*, 7192 – 7197.
[14] C. Wiesmann, G. Fuh, H. W. Christinger, C. Eigenbrot, J. A. Wells, A. M. de Vos, *Cell* **1997**, *91*, 695 – 704.
[15] W. J. Fairbrother, M. A. Champe, H. W. Christinger, B. A. Keyt, M. A. Starovasnik, *Protein Sci.* **1997**, *6*, 2250 – 2260.
[16] G. Niu, X. Chen, *Curr. Drug Targets* **2010**, *11*, 1000 – 1017.
[17] J. E. Nör, J. Christensen, D. J. Mooney, P. J. Polverini, *Am. J. Pathol.* **1999**, *154*, 375 – 384.
[18] A. Hoeben, B. Landuyt, M. S. Highley, H. Wildiers, A. T. Van Oosterom, E. A. De Bruijn, *Pharmacol. Rev.* **2004**, *56*, 549 – 580.
[19] R. Kerbel, J. Folkman, *Nat. Rev. Cancer* **2002**, *2*, 727 – 739.
[20] L. M. Ellis, D. J. Hicklin, *Nat. Rev. Cancer* **2008**, *8*, 579 – 591.
[21] D. S. Boyer, J. J. Hopkins, J. Sorof, J. S. Ehrlich, *Ther. Adv. Endocrinol. Metab.* **2013**, *4*, 151 – 169.
[22] R. K. Jain, *Cancer Cell* **2014**, *26*, 605 – 622.
[23] P. K. Kaiser, *Ophthalmology* **2013**, *120*, S11 – S15.
[24] R. J. Motzer, T. E. Hutson, P. Tomczak, D. Michaelson, R. M. Bukowski, O. Rixe, S. Oudard, S. Negrier, C. Szczylik, S. T. Kim, I. Chen, P. W. Bycott, C. M. Baum, R. A. Figlin, *N. Engl. J. Med.* **2007**, *356*, 115 – 124.
[25] E. Raymond, L. Dahan, J. L. Raoul, Y. J. Bang, I. Borbath, C. Lombard-Bohas, J. Valle, P. Metrakos, D. Smith, A. Vinik, *N. Engl. J. Med.* **2011**, *364*, 501 – 513.
[26] B. Escudier, T. Eisen, W. M. Stadler, C. Szczylik, S. Oudard, M. Siebels, S. Negrier, C. Chevreau, E. Solska, A. A. Desai, *N. Engl. J. Med.* **2007**, *356*, 125 – 134.
[27] J. M. Llovet, S. Ricci, V. Mazzaferro, P. Hilgard, E. Gane, J. F. Blanc, A. C. de Oliveira, A. Santoro, J. L. Raoul, A. Forner, *N. Engl. J. Med.* **2008**, *359*, 378 – 390.
[28] C. N. Sternberg, I. D. Davis, J. Mardiak, C. Szczylik, E. Lee, J. Wagstaff, C. H. Barrios, P. Salman, O. A. Gladkov, A. Kavina, *J. Clin. Oncol.* **2010**, *28*, 1061 – 1068.
[29] W. T. A. van der Graaf, J.-Y. Blay, S. P Chawla, D.-W. Kim, B. Bui-Nguyen, P. G. Casali, P. Schöffski, M. Aglietta, A. P. Staddon, Y. Beppu, A. Le Cesne, H. Gelderblom, I. R. Judson, N. Araki, M. Ouali, S. Marreaud, R. Hodge, M. R. Dewji, C. Coens, G. D. Demetri, C. D. Fletcher, A. P. Dei Tos, P. Hohenberger, *Lancet* **2012**, *379*, 1879 – 1886.
[30] S. A. Wells Jr., B. G. Robinson, R. F. Gagel, H. Dralle, J. A. Fagin, M. Santoro, E. Baudin, R. Elisei, B. Jarzab, J. R. Vasselli, *J. Clin. Oncol.* **2012**, *30*, 134 – 141.
[31] R. J. Motzer, B. Escudier, P. Tomczak, T. E. Hutson, M. D. Michaelson, S. Negrier, S. Oudard, M. E. Gore, J. Tarazi, S. Hariharan, *Lancet Oncol.* **2013**, *14*, 552 – 562.
[32] A. Grothey, E. Van Cutsem, A. Sobrero, S. Siena, A. Falcone, M. Ychou, Y. Humblet, O. Bouché, L. Mineur, C. Barone, A. Adenis, J. Tabernero, T. Yoshino, H.-J. Lenz, R. M. Goldberg, D. J. Sargent, F. Cihon, L. Cupit, A. Wagner, D. Laurent, *Lancet* **2013**, *381*, 303 – 312.
[33] R. Elisei, M. J. Schlumberger, S. P. Müller, P. Schöffski, M. S. Brose, M. H. Shah, L. Licitra, B. Jarzab, V. Medvedev, M. C. Kreissl, *J. Clin. Oncol.* **2013**, *31*, 3639 – 3646.
[34] H. L. Kindler, D. Niedzwiecki, D. Hollis, S. Sutherland, D. Schrag, H. Hurwitz, F. Innocenti, M. F. Mulcahy, E. O'Reilly, T. F. Wozniak, *J. Clin. Oncol.* **2010**, *28*, 3617 – 3622.
[35] H. Wilke, K. Muro, E. Van Cutsem, S. C. Oh, G. Bodoky, Y. Shimada, S. Hironaka, N. Sugimoto, O. Lipatov, T.-Y. Kim, *Lancet Oncol.* **2014**, *15*, 1224 – 1235.
[36] C. S. Fuchs, J. Tomasek, C. J. Yong, F. Dumitru, R. Passalacqua, C. Goswami, H. Safran, L. V. dos Santos, G. Aprile, D. R. Ferry, B. Melichar, M. Tehfe, E. Topuzov, J. R. Zalcberg, I. Chau, W. Campbell, C. Sivanandan, J. Pikiel, M. Koshiji, Y. Hsu, A. M. Liepa, L. Gao, J. D. Schwartz, J. Tabernero, *Lancet* **2014**, *383*, 31 – 39.
[37] E. Van Cutsem, J. Tabernero, R. Lakomy, H. Prenen, J. Prausová, T. Macarulla, P. Ruff, G. A. van Hazel, V. Moiseyenko, D. Ferry, J. McKendrick, J. Polikoff, A. Tellier, R. Castan, C. Allegra, *J. Clin. Oncol.* **2012**, *30*, 3499 – 3506.
[38] E. W. Ng, D. T. Shima, P. Calias, E. T. Cunningham, D. R. Guyer, A. P. Adamis, *Nat. Rev. Drug Discovery* **2006**, *5*, 123 – 132.
[39] B. Gautier, M. A. Miteva, V. Goncalves, F. Huguenot, P. Coric, S. Bouaziz, B. Seijo, J. F. Gaucher, I. Broutin, C. Garbay, A. Lesnard, S. Rault, N. Inguimbert, B. O. Villoutreix, M. Vidal, *Chem. Biol.* **2011**, *18*, 1631 – 1639.
[40] B. Pan, B. Li, S. J. Russell, J. Y. Tom, A. G. Cocharan, W. J. Fairbrother, *J. Mol. Biol.* **2002**, *316*, 769 – 787.
[41] M. Mayer, B. Meyer, *Angew. Chem. Int. Ed.* **1999**, *38*, 1784 – 1788; *Angew. Chem.* **1999**, *111*, 1902 – 1906.
[42] C. Dalvit, P. Pevarello, M. Tato, M. Veronesi, A. Vulpetti, M. Sundström, *J. Biomol. NMR* **2000**, *18*, 65 – 68.
[43] H. Tang, Y. Wang, J. K. Nicholson, J. C. Lindon, *Anal. Biochem.* **2004**, *325*, 260 – 272.
[44] C. Dalvit, *Prog. Nucl. Magn. Reson. Spectrosc.* **2007**, *51*, 243 – 271.
[45] M. S. Brozzo, S. Bjelić, K. Kisko, T. Schleier, V.-M. Leppänen, K. Alitalo, F. K. Winkler, K. Ballmer-Hofer, *Blood* **2012**, *119*, 1781 – 1788.
[46] J. W. Checco, D. F. Kreitler, N. C. Thomas, D. G. Belair, N. J. Rettko, W. L. Murphy, K. T. Forest, S. H. Gellman, *Proc. Natl. Acad. Sci. USA* **2015**, *112*, 4552 – 4557.
[47] H. S. Haase, K. J. Peterson-Kaufman, S. K. Lan Levengood, J. W. Checco, W. L. Murphy, S. H. Gellman, *J. Am. Chem. Soc.* **2012**, *134*, 7652 – 7655.
[48] W. A. Hendrickson, J. R. Horton, D. M. LeMaster, *EMBO J.* **1990**, *9*, 1665 – 1672.
[49] R. Otten, J. Villali, D. Kern, F. A. Mulder, *J. Am. Chem. Soc.* **2010**, *132*, 17004 – 17014.
[50] E. R. London, W. E. Wageman, R. L. Blakley, *FEBS Lett.* **1983**, *160*, 56 – 60.
[51] Z. Serber, W. Straub, L. Corsini, A. M. Nomura, N. Shimba, C. S. Craik, P. Ortiz de Montellano, V. Dötsch, *J. Am. Chem. Soc.* **2004**, *126*, 7119 – 7125.
[52] A. Dyachenko, M. Goldflam, M. Vilaseca, E. Giralt, *Biopolymers* **2010**, *94*, 689 – 700.
[53] R. Prades, R. B. Oller-Salvia, S. M. Schwarzmaier, J. Selva, M. Moros, M. Balbi, V. Grazú, J. M. de La Fuente, G. Egea, G. N. Plesnila, M. Teixidó, E. Giralt, *Angew. Chem. Int. Ed.* **2015**, *54*, 3967 – 3972; *Angew. Chem.* **2015**, *127*, 4039 – 4044.
[54] C. J. Hipolito, H. Suga, *Curr. Opin. Chem. Biol.* **2012**, *16*, 196 – 203.
[55] Y. Goto, T. Katoh, H. Suga, *Nat. Protoc.* **2011**, *6*, 779 – 790.
[56] H. Murakami, A. Ohta, H. Ashigai, H. Suga, *Nat. Methods* **2006**, *3*, 357 – 359.
[57] Y. Goto, H. Suga, *Methods Mol. Biol.* **2012**, *848*, 465 – 478.
[58] Y. Sako, J. Morimoto, H. Murakami, H. Suga, *J. Am. Chem. Soc.* **2008**, *130*, 7232 – 7234.
[59] Y. Goto, H. Murakami, H. Suga, *RNA* **2008**, *14*, 1390 – 1398.
[60] Y. Goto, A. Ohta, Y. Sako, Y. Yamagishi, H. Murakami, H. Suga, *ACS Chem. Biol.* **2008**, *3*, 120 – 129.
[61] T. Kawakami, H. Murakami, H. Suga, *Chem. Biol.* **2008**, *15*, 32 – 42.
[62] T. Kawakami, H. Murakami, H. Suga, *J. Am. Chem. Soc.* **2008**, *130*, 16861 – 16863.
[63] K. J. Peterson, J. D. Sadowsky, E. A. Scheef, S. Pal, K. D. Kourentzi, R. C. Willson, E. H. Bresnick, N. Sheibani, S. H. Gellman, *Anal. Biochem.* **2008**, *378*, 8 – 14.
[64] M. Fischer, R. E. Hubbard, *Mol. Interventions* **2009**, *9*, 22 – 30.
[65] R. S. Bohacek, C. McMartin, W. C. Guida, *Med. Res. Rev.* **1996**, *16*, 3 – 50.
[66] L. C. Blum, J. L. Reymond, *J. Am. Chem. Soc.* **2009**, *131*, 8732 – 8733.

[67] R. E. Hubbard, *J. Synchrotron Radiat.* **2008**, *15*, 227 – 230.
[68] X. Arroyo, M. Goldflam, M. Feliz, I. Belda, E. Giralt, *PLOS ONE* **2013**, *8*, e58571.
[69] M. Garavís, B. López-Méndez, A. Somoza, J. Oyarzabal, C. Dalvit, A. Villasante, R. Campos-Olivas, C. González, *ACS Chem. Biol.* **2014**, *9*, 1559 – 1566.
[70] Schrödinger Release 2013-3, Schrödinger Suite 2013 Protein Preparation Wizard: Epik version 2.6, Impact version 6.1, Prime version 3.4, SiteMap version 2.9, LigPrep version 2.8, Glide version 6.1; Schrödinger LLC, New York, NY (USA), **2013**.
[71] K. W. Borrelli, A. Vitalis, R. Alcantara, V. Guallar, *J. Chem. Theory Comput.* **2005**, *1*, 1304 – 1311.
[72] D. R. Yance, S. M. Sagar, *Integr. Cancer Ther.* **2006**, *5*, 9 – 29.
[73] D. J. Newman, M. C. Gordon, *J. Nat. Prod.* **2012**, *75*, 311 – 335.
[74] C. Liu, A. Tseng, S. Yang, *Chinese Herbal Medicine: Modern Applications of Traditional Formulas*, CRC Press, Boca Raton, **2005**.
[75] S. Ikemoto, K. Sugimura, N. Yoshida, R. Yasumoto, S. Wada, K. Yamamoto, T. Kishimoto, *Urologia* **2000**, *55*, 951 – 955.
[76] C. M. Crews, *Chem. Biol.* **2010**, *17*, 551 – 555.
[77] C. F. Cheok, C. S. Verma, J. Baselga, D. P. Lane, *Nat. Rev. Clin. Oncol.* **2011**, *8*, 25 – 37.
[78] A. M. Petros, J. Dinges, D. J. Augeri, S. A. Baumeister, D. A. Betebenner, M. G. Bures, S. W. Elmore, P. J. Hajduk, M. K. Joseph, S. K. Landis, D. G. Nettesheim, S. H. Rosenberg, W. Shen, S. Thomas, X. Wang, I. Zanze, H. Zhang, S. W. Fesik, *J. Med. Chem.* **2006**, *49*, 656 – 663.
[79] A. C. Braisted, J. D. Oslob, W. L. Delano, J. Hyde, R. S. McDowell, N. Waal, C. Yu, M. R. Arkin, B. C. Raimundo, *J. Am. Chem. Soc.* **2003**, *125*, 3714 – 3715.
[80] L. Nevola, E. Giralt, *Chem. Commun.* **2015**, *51*, 3302 – 3315.
[81] A. Martín-Quirós, L. Nevola, K. Eckelt, S. Madurga, P. Gorostiza, E. Giralt, *Chem. Biol.* **2015**, *22*, 31 – 37.
[82] M. Goldflam, T. Tarragó, M. Gairí, E. Giralt, *Methods Mol. Biol.* **2012**, *831*, 233 – 259.

Received: October 9, 2015
Published online on November 10, 2015

